Environmental Science Nano

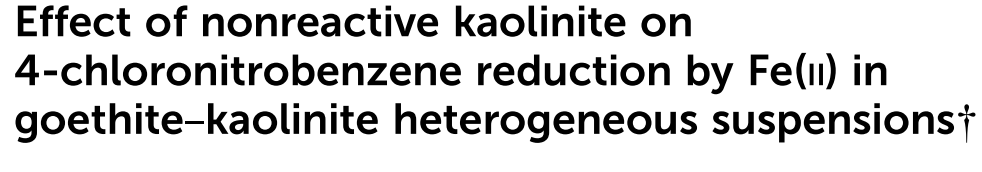


PAPER

View Article Online
View Journal | View Issue



Cite this: Environ. Sci.: Nano, 2017, 4. 325



Jennifer H. Strehlau,^a Jonathan D. Schultz,^a Amanda M. Vindedahl,^a William A. Arnold*^b and R. Lee Penn*^a

The kinetics of model contaminant 4-chloronitrobenzene (4-ClNB) reduction by Fe(n) in aqueous suspensions containing either or both goethite (α -FeOOH) nanoparticles and kaolinite ($Al_2Si_2O_5(OH)_4$) were quantified to elucidate the effects of nonreactive clay minerals on the attenuation of nitroaromatic groundwater contaminants by iron oxide nanoparticles. Increasing the amount of kaolinite in the presence of goethite decreased the reduction rate of 4-ClNB and competitive Fe(n) adsorption on kaolinite occurred. Cryogenic transmission and scanning electron microscopy (cryo-TEM and cryo-SEM) images did not reveal significant loss of accessible reactive surface area as a result of heteroaggregation. Sequential-spike batch reactors revealed that in the presence of kaolinite, 4-ClNB reduction rate decreased by more than a factor of three with extended reaction as a result of kaolinite dissolution and subsequent incorporation of Al and Si in goethite or on the goethite surface. The reactive sites residing on the {110} faces were comparatively more reactive in the presence of a large loading of kaolinite, resulting in shorter and wider goethite particles after reaction. These results elucidate the mechanisms by which nonreactive clays affect the reactions of Fe(n)/ iron oxides in groundwater systems and indicate that nonreactive clays are not passive components.

Received 8th October 2016, Accepted 21st December 2016

DOI: 10.1039/c6en00469e

rsc.li/es-nano

Environmental significance

Natural attenuation of nitroaromatic groundwater contaminants may involve anaerobic, abiotic redox reactions at the iron oxide-water interface, with goethite nanoparticles of particular interest due to their high specific surface areas and abundance in groundwater systems. In an effort to elucidate the effects of nonreactive clays on these reactions, kaolinite was added to $Fe(\pi)/g$ oethite reactors and then reacted with one to five spikes of model contaminant 4-chloronitrobenzene (4-ClNB). The presence of kaolinite, which did not reduce 4-ClNB directly or mediate 4-ClNB reduction in the presence of $Fe(\pi)/g$ oethite reactivity. These results demonstrate that even nonreactive minerals may influence outcomes of natural attenuation in groundwater that contains iron oxide nanoparticles.

minerals.8,12-17

Introduction

E-mail: arnol032@umn.edu

Abiotic chemical reduction by $Fe(\pi)$ associated with iron oxide nanoparticle surfaces has been investigated for decades as a process for natural attenuation of groundwater threatened by anthropogenic contaminants, including nitroaromatic compounds (NACs) such as certain explosives and pesticides. These reactions are driven by interfacial electron transfer between $Fe(\pi)$ and structural $Fe(\pi)$ at the

mineral-water interface, where sorption of aqueous Fe(II) on the surface of an Fe(III)-containing mineral creates a reactive

site for NAC reduction.⁴ Because clay minerals are commonly found in sediments that are also rich with iron oxides,⁵ understanding how heterogeneous clay–iron oxide mixtures affect redox reactions at the iron oxide–water interface is important for predicting outcomes of natural attenuation in the environment. Certain clay minerals, particularly those containing structural Fe species, directly serve as reductants of NACs in the presence of aqueous Fe(n).^{6–11} Due to their potential for natural attenuation processes in contaminated groundwater, Fe-rich clays, such as substituted nontrolites and smectites, have been studied in great detail. For example, recent spectroscopic and electrochemical studies have revealed details at the molecular level, elucidating Fe(n)–Fe(m) electron transfer and redox properties of clay

^a Department of Chemistry, University of Minnesota, 207 Pleasant Street SE, Minneapolis, Minnesota, 55455-0431, USA. E-mail: rleepenn@umn.edu ^b Department of Civil, Environmental, and Geo-Engineering, University of Minnesota, 500 Pillsbury Drive SE, Minneapolis, Minnesota, 55455-0116, USA.

 $[\]dagger$ Electronic supplementary information (ESI) available. See DOI: 10.1039/c6en00469e

On the other hand, the mechanisms by which nonreactive clays, such as kaolinite $(Al_2Si_2O_5(OH)_4)$ in its unsubstituted form) and other clays that contain trace or no redox active cations, affect the redox reactions of Fe(II) in mixed mineral suspensions with iron oxides have not yet been studied. Potential mechanisms include sequestration of available NAC or Fe(II) by sorption onto the nonreactive mineral surface, alteration or poisoning of reactive surfaces by dissolved species produced by clay dissolution, or decrease of accessible surface area of reactive surfaces by way of heteroaggregation.

Adsorption processes on clay minerals have been the subject of much research, given their potential to sequester organic contaminants and heavy metals in the subsurface. NAC sorption on smectites 18–20 and substituted kaolinites 21,22 has been demonstrated, and kaolinite has also been described as an effective adsorbent for a range of ions, 23 including Fe(II). Co-adsorption of various ions (*e.g.*, phosphate, Pb(II)) has also been modeled and experimentally determined for kaolinite in the presence of iron oxide minerals, 25–27 but Fe(II) adsorption in iron oxide–kaolinite heterogeneous systems has not been presented.

Dissolution of clay minerals and release of dissolved ions are also possible at circumneutral pH.28 The release of Al and Si ions would alter the solution chemistry, and the presence of Al and Si ions during iron oxide growth has been shown to affect the size, morphology, and composition of resulting particles by incorporation into the crystal matrix, which may alter the relative reactivity of iron oxide surfaces for reduction of NACs by Fe(II). 29,30 For instance, Jones et al. recently described the loss of reactivity in NAC reduction by Fe(II) mediated with Si-doped ferrihydrite nanoparticles as compared to pure ferrihydrite.³¹ Frierdich et al. described the inhibition of Fe(II) sorption on the goethite surface due to Al substitution in the goethite bulk structure, which would decrease the number of reactive surface sites for NAC reduction by sorbed Fe(II).³² Both of these studies suggest that nonreactive aluminosilicate clays may indirectly affect redox reactions at the iron oxide mineral surface through production of dissolved Al and Si species. The Al and Si could then be incorporated into the goethite crystal during oxidative growth or recrystallization in the presence of Fe(II).³³

Lastly, heteroaggregation, or the formation of aggregates composed of a heterogeneous mineral mixture, could decrease the number of accessible reactive surface sites. 34-36 Points of zero charge depend on various factors, but iron oxides are generally neutral at pH 6-9 and kaolinite at pH 3-4. 37,38 At circumneutral pH, therefore, these two minerals could be expected to heteroaggregate based on attractive surface charges. The best technique for directly imaging aggregates as they exist in aqueous suspension is cryogenic microscopy, 39 such as cryogenic transmission and scanning electron microscopy (cryo-TEM and cryo-SEM). Cryogenic microscopy has been previously used to study aggregation in aqueous suspensions of iron oxide particles, 40,41 but few have imaged mixed iron oxide-clay suspensions in their native state using cryo-SEM. 42 At this time, no studies have been

found that provide cryo-TEM images of clay-iron oxide suspensions in dilute aqueous solutions with chemistry similar to groundwater.

While a great deal of effort has gone into describing redox active clays and their surface-mediated reactions with contaminants, it is clear that much work is needed to elucidate the role of nonreactive clays. The objectives of this work were to determine whether kaolinite influences the surfacemediated redox reactions of Fe(II) in the presence of goethite (α-FeOOH) nanoparticles and to elucidate the mechanisms by which nonreactive clays affect these reactions. The kinetics of 4-chloronitrobenzene (4-ClNB) reduction by Fe(II) in suspensions containing either or both goethite and kaolinite were quantified. Cryogenic SEM and TEM were used to examine the aggregation state of the suspended mineral particles. The oxidative growth of goethite was quantified from calibrated TEM images and the relative rates of growth along and perpendicular to the long axis of the goethite particles were determined. These results, coupled with elemental analysis of supernatants and goethite particles, demonstrate that the most important control parameter is the solution chemistry, with dissolved species generated by partial dissolution of the kaolinite particles serving to alter the relative reactivity of goethite crystal faces. The findings offer novel insight into how nonreactive clay minerals impact the reactivity of Fe(II) with NACs in heterogeneous suspensions also containing iron oxides.

Experimental section

Materials

Chemicals were purchased from the following sources: FeCl₂ ·4H2O, NaOH, methanol, and acetonitrile from Fisher, HCl from BDH Aristar, ammonium acetate and H2SO4 from Mallinckrodt, NaHCO₃ from Sigma Aldrich, and ferrozine from Alfa Aesar. All solvents were HPLC grade. Ultrapure water (18.2 M Ω cm, Milli-Q) was the only water source used. Acrodisc syringe filters (0.2 µm nylon membrane) were purchased from Pall Life Sciences. Goethite nanoparticles were prepared by the method of Anschutz and Penn and stored at 4 °C in ultrapure water with an experimentally determined mass loading of 15.1 g L⁻¹.43 Well-crystallized kaolinite (KGa-1b, Washington County, Georgia) was purchased from The Clay Mineral Society with characterization provided by Pruett and Webb. 44 Kaolinite stock suspensions were prepared fresh by weighing kaolinite in 20 mL scintillation vials and diluting with ultrapure water. A concentrated stock (80 g L⁻¹) was used for preparation of reactors with high kaolinite loadings. When the desired mass loading was low, a dilute stock (8 g L^{-1}) was prepared by diluting the concentrated stock. To quantify mass loading, five aliquots were delivered to weigh boats, dried at room temperature, and weighed to ensure that the delivered volume provided the expected mass.

Single-spike reactors

All reactions were performed in an anaerobic environment (Coy glovebag, 95% $N_2/5\%$ H_2 , <1 ppm O_2), and reactors

were prepared using freshly made 10 mM bicarbonate buffer at pH 7 made by adding 0.840 g NaHCO3 to 1 L ultrapure water and adjusting pH with 1 M H₂SO₄. Five 120 mL glass reactors were prepared: one with no minerals, one with 0.325 g L⁻¹ kaolinite, one with 0.325 g L⁻¹ goethite, and two mixed mineral suspensions with 0.325 g L⁻¹ goethite and either 0.05 or 2 g L⁻¹ kaolinite. The final reactor volume was 120 mL. The general procedure for reactor preparation included adding the appropriate volume of goethite stock suspension to the reactors, followed by the necessary volume of kaolinite stock suspension. Bicarbonate buffer was added to reach 118 mL, and the reactors were immediately capped with Teflon plugs to prevent outgassing. To each reactor, 0.69 mL of a fresh stock solution of 175 mM Fe(II) made from FeCl₂·4H₂O in 30 mM HCl was added (reactor concentration of 1 mM $Fe(\pi)$). After the reactors were magnetically stirred for 21–24 hours, the pH was recorded and 1.2 mL of 10 mM 4-ClNB in methanol was added to initiate the reaction (initial reactor concentration of 0.1 mM 4-ClNB). After the initial spike of 4-ClNB, samples were withdrawn periodically over 2 h using a plastic syringe and filtered through 13 mm Acrodisc filters with 0.2 μm nylon membrane into amber glass HPLC vials. An Agilent 1100 Series system with UV detector and Zorbax SB-C18 column (4.6 mm × 150 mm, 5 μm) was used to quantify 4-ClNB concentration from a five-point calibration curve (0.02-0.1 mM). HPLC parameters included a 20 µL injection, 70% acetonitrile and 30% ammonium acetate in water (1 g L⁻¹, pH 7) mobile phase, detection wavelength of 254 nm, and 7 min separation time.

To test the effect of kaolinite dissolution, fresh kaolinite stock suspension was prepared using water. After one day and seven days, aliquots of the suspension were filtered using 0.2 μm Nylon membrane filters. The resulting filtrate was added to reaction in lieu of the stock kaolinite suspension, and the rate of 4-ClNB loss was quantified as with the previously described experiments.

Fe(II) quantification

Fe(II) adsorption was determined by quantifying dissolved Fe(II) in filtrates of suspensions after 21 h equilibration time using a ferrozine colorimetric assay. 45 Prior to 4-ClNB addition, 1 mL of suspension was removed from each reactor and filtered. To quantify dissolved Fe(11), 0.2 mL of filtrate, 2.4 mL of water, and 0.2 mL of ferrozine stock solution (5 mg mL⁻¹ in ultrapure water) were added in a 1 cm polystyrene cuvette. Each cuvette was capped, inverted three times, removed from the glovebag, and analyzed with an Agilent 8452 UV-visible spectrometer at 562 nm. Aqueous Fe(II) was quantified using a five-point calibration curve (0.01-0.08 mM), and average adsorbed Fe(II) was calculated by difference between controls that contained no particles and resultant aqueous Fe(II) from three trials. For adsorption isotherms, separate vials containing various mass loadings (0-2 g L-1) of goethite or kaolinite were prepared anaerobically in the bicarbonate buffer (15 mL total volume). To each vial, 0.2 mL of 175 mM

Fe(II) was spiked and equilibrated for 21 h before samples (\sim 1 mL) were withdrawn and filtered. The filtrate was analyzed by UV-vis as described above.

Sequential-spike batch reactors

Triplicate sequential-spike batch reactors were prepared in a process similar to the single-spike experiments. Two mixed mineral systems were tested, 0.05 or 2 g $\rm L^{-1}$ kaolinite with 0.325 g $\rm L^{-1}$ goethite, for a total of six reactors for one trial (3 reactors \times 2 mass loadings). The sequential-spike process is detailed in our previous work. 46

Filtrates of suspensions from both kaolinite loadings after one and five spikes of 4-ClNB were analyzed by inductively coupled plasma optical emission spectroscopy (ICP-OES) to quantify dissolved Si and Al concentrations. Additionally, a separate experiment involved adding 0.325 g L⁻¹ goethite and 1 mM Fe(II) to a 250 mL Erlenmeyer flask, diluted to 200 mL with bicarbonate buffer. Then, 20 mL of a 22 g L⁻¹ kaolinite suspension in the same bicarbonate buffer was loaded into dialysis tubing, sealed using dialysis clips, and submerged in the goethite suspension. The flask was capped and stirred magnetically inside the glovebag. After 14 d, ~5 mL of the goethite suspension was filtered for ICP-OES analysis. The solid goethite was collected as described below, dissolved, and analyzed by ICP-OES. Major elemental analyses of filtrates and solids were performed using a Thermo Scientific iCAP 6500 duo optical emission spectrometer with simultaneous charge induction detection from five replicate sample injections. Samples were acidified prior to analysis, and an internal standard of yttrium was added.

Solid collection and characterization

Solid collection consisted of centrifuging (7000 rpm for 3 min), washing (3×20 mL ultrapure water), and air drying the particles. Post-reaction solids for goethite reactors containing 0.05 or 2 g L⁻¹ kaolinite after five spikes of 4-ClNB were characterized by low-temperature magnetic characterization (10–300 K) on a Quantum Designs Magnetic Property Measurement System (MPMS) cryogenic magnetometer (10^{-10} A m² sensitivity) with a 2.5 T applied field for field cooled-zero field cooled (FC-ZFC) analyses.

Microscopy

Conventional TEM was performed using a FEI Tecnai T12 TEM microscope operated at 120 kV equipped with a LaB₆ electron source and Gatan charge-coupled device (CCD) camera. Samples were prepared by diluting $\sim\!10~\mu\text{L}$ of reactor suspension to 1 mL with ultrapure water, sonicating for 20 s, and air-drying a single drop on a holey carbon 200 mesh copper grid (SPI Supplies). Goethite length and width measurements ($\sim\!500$ particles per sample) were collected from a minimum of 20 calibrated images collected at 4 different grid locations using ImageJ (National Institute of Health, v1.47). Cryo-TEM was performed using a FEI Technai G^2 Spirit BioTWIN TEM equipped with a LaB₆ source and Eagle 2 k CCD

camera. Grids were prepared by placing $\sim 3~\mu L$ of sample onto a 3 mm 200-mesh lacey carbon coated copper grid (SPI Supplies), blotting with filter paper for 1 s using a Vitrobot Mark IV (FEI), plunging into liquid ethane, and transferring to a cryo-TEM holder under liquid nitrogen. Grids were imaged at 120 kV on a cryo stage.

Conventional SEM was performed on a Hitachi S-4700 SEM microscope with cold field emission gun at 3 kV. Samples were prepared by drying a drop of the reactor suspension directly onto copper tape. Cryo-SEM was performed on the same microscope, imaged at 3 kV and -160 °C. Samples for cryo-SEM were prepared by placing a drop of suspension onto a Si wafer chip $(5 \times 7 \text{ mm})$ that was previously scored in the center and cleaned by 30 s of plasma glow discharge in a DV-502A Denton Vacuum system. The chip was then manually plunged into liquid ethane and transferred immediately to liquid nitrogen. Under liquid nitrogen, the chip was placed into a cryo-SEM sample holder and cracked in half along the score with precooled tweezers, revealing a cross section of the sample. The sample holder was then cryogenically transferred to an Emitech K-1250 Cryo Preparation Unit, sublimed at -96 °C for 10 min, sputtered with Pt (\sim 2 nm layer), and transferred to the microscope for imaging.

Results and discussion

Effect of kaolinite on initial 4-ClNB reduction by Fe(II)/goethite

Pseudo first-order rate constants $(k_{\rm obs})$ for 4-ClNB reduction by Fe(II) in the goethite-containing reactors are provided in Table 1. Reduction rate of the first spike of 4-ClNB by adsorbed Fe(II) on goethite was significantly slower in the presence of 2 g L⁻¹ kaolinite. Three viable hypotheses that could explain the decrease in reactivity are adsorption of 4-ClNB and/or Fe(II) onto kaolinite, which may limit the availability of 4-ClNB and/or Fe(II) at the goethite—water interface; heteroaggregation, which could effectively sequester some goethite surface area from the aqueous medium; and kaolinite dissolution, which would result in the production of dissolved species that could interfere with Fe(II) adsorption or oxidation.

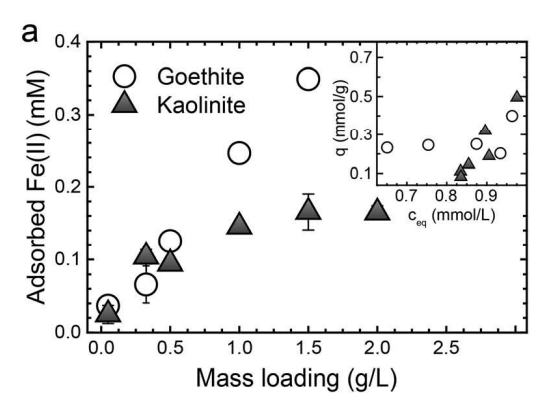
Adsorption of 4-ClNB onto kaolinite was not detected, and reactors containing no particles or only kaolinite with 4-ClNB and Fe(II) were relatively unreactive (ESI;† Fig. S1), evidence that Fe(II) adsorbed on the goethite surface was the only reductant of 4-ClNB. Kaolinite dissolution and the release of Al and Si ions has been previously observed and kinetically modeled at circumneutral pH.^{28,47,48} In the present study, the kinetics of 4-ClNB loss was monitored in a reactor containing Fe(II), goethite, and the filtrate from the kaolinite stock suspension (Fig. S2†). When the filtrate was collected from a fresh kaolinite stock suspension, no differences in reactivity were observed as compared to the reference condition (reactors containing only Fe(II) and goethite). When the filtrate was collected from a kaolinite suspension that was seven days old, a slight but significant decrease in reaction rate was observed. Thus, kaolinite dissolution over time and resultant variations in solution chemistry could influence Fe(II)/ goethite reactivity for aged systems, such as in the sequentialspike experiments or natural environmental settings, but not in the single-spike reactions, which were freshly prepared and reacted in under two days.

Competitive Fe(II) adsorption between goethite and kaolinite was quantified through adsorption isotherms and measurement of adsorbed Fe(II) in the reactors (Fig. 1). Adsorption isotherms (Fig. 1a) as a function of particle mass loading revealed that Fe(II) adsorbed onto both goethite and kaolinite in the 10 mM bicarbonate buffer at pH 7. The amount of adsorbed Fe(II) per goethite mass was independent of equilibrium aqueous Fe(II) concentration (Fig. 1a inset), evidence that the goethite surface was saturated with $Fe(\pi)$. In contrast, q_{max} was not reached in kaolinite suspensions, and the nonlinear relationship between adsorbed Fe(II) and kaolinite loading may be due to flocculation in the suspensions. Reactors with only goethite and with goethite and 0.05 g L^{-1} kaolinite had similar total adsorption capacities for Fe(II) (Fig. 1b). When kaolinite loading was increased to 2 g L^{-1} , the amount of adsorbed Fe(II) increased, consistent with coadsorption of Fe(II) onto goethite and kaolinite. Competitive adsorption of Fe(II) on kaolinite could influence the competition for reactive sites on goethite, thereby decreasing the

Table 1 Average pseudo-first order rates for 4-CINB reduction by Fe(II) adsorbed on goethite and resultant length and width measurements of goethite

Sample	Stage	$k_{\mathrm{obs}}^{}a}\left(\mathbf{h}^{-1}\right)$	$\operatorname{Length}^{b}\left(\operatorname{nm}\right)$	$\operatorname{Width}^b(\operatorname{nm})$	N	$[Si]^c$ (ppm)	$[Al]^c$ (ppm)	Reaction time (d)
Initial	Before reaction	NA	110 ± 41	12 ± 5	500	0.2 wt%	0 wt%	NA
$G_{0.325}$	Spike 1	0.75 ± 0.04	_	_	_	3.0	0.06	1^d
$G_{0.325}K_{0.05}$	Spike 1	0.74 ± 0.04	_	_	_	0.5	0	1
	Spike 3	0.42 ± 0.04	146 ± 46	12 ± 5	500	_	_	6
	Spike 5	0.26 ± 0.01	177 ± 56	13 ± 4	405	3.0	0.04	18
$G_{0.325}K_2$	Spike 1	0.55 ± 0.05	_	_	_	3.2	0	1
	Spike 3	0.11 ± 0.01	133 ± 41	14 ± 4	413	_	_	11
	Spike 5	0.069 ± 0.006	157 ± 46	18 ± 4	473	6.3	0.05	30

^a Rate constants were determined by linear regression, where errors are the 95% confidence intervals and R^2 values were greater than 0.98. Reactions were performed in 10 mM bicarbonate buffer at pH 7 with initial Fe(II) concentration of 1 mM. Sample notation indicates the mass loading of goethite (G) or kaolinite (K) in g L⁻¹. ^b Errors are the standard deviations. ^c Concentrations of Si and Al analyzed by ICP-OES were filtrates, with the exception of the initial particles (solids, wt% provided). ^d Reaction was complete after 1 d and then stirred 17 d to match total time of $G_{0.325}K_{0.05}$ experiments. N = number of measured particles. NA = not applicable. No data = not measured.



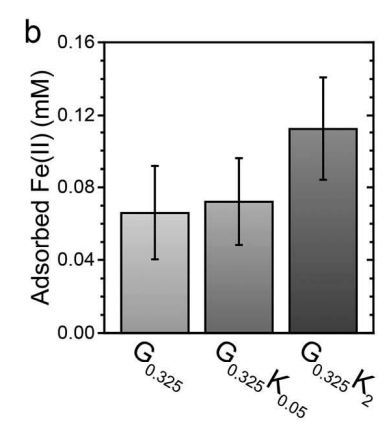


Fig. 1 a) Fe(II) adsorption isotherms on either goethite or kaolinite as a function of particle mass loading. Inset shows the same data described by q (adsorbed Fe(II) per mass of sorbent) as a function of c_{eq} (aqueous Fe(II) concentration). b) Adsorbed Fe(II) in systems containing various mineral loadings. Sample notation indicates the mass loading of goethite (G) or kaolinite (K) in g L^{-1} . Error bars are the standard deviations from triplicate trials. Both studies were performed in 10 mM bicarbonate buffer at pH 7 with an initial Fe(II) concentration of 1 mM.

reaction kinetics of 4-ClNB reduction. Although Fe(II) adsorbed onto kaolinite, it was still relatively unreactive towards 4-ClNB (Fig. S2†). In contrast, Klausen et al. described the detectable reactivity of Fe(II) on kaolinite towards similar NACs. The difference between the study described here and that of Klausen et al. could be the different solution conditions (including pH and buffer identity). Another possibility is the source of kaolinite (i.e., extent of iron isomorphic substitution) and/or the production of an iron oxide coating as stated in Klausen et al., both of which would lead to increased NAC reduction rates. The results shown in this study

demonstrate that certain kaolinite samples can serve as nonreactive competitors for Fe(II) sorption in a heterogeneous mineral system, thereby influencing overall rates of reduction by reducing the number of Fe(II) species on the iron oxides.

Finally, heteroaggregation is possible and also promoted given that the net surface charges of goethite (positive) and kaolinite (negative) are attractive at pH 7. It has been shown that goethite aggregation influences Fe(II) reactivity, 49 but heteroaggregation in mineral mixtures is less characterized. Fig. 2a and b show representative images using conventional SEM and TEM, respectively. While it appeared that

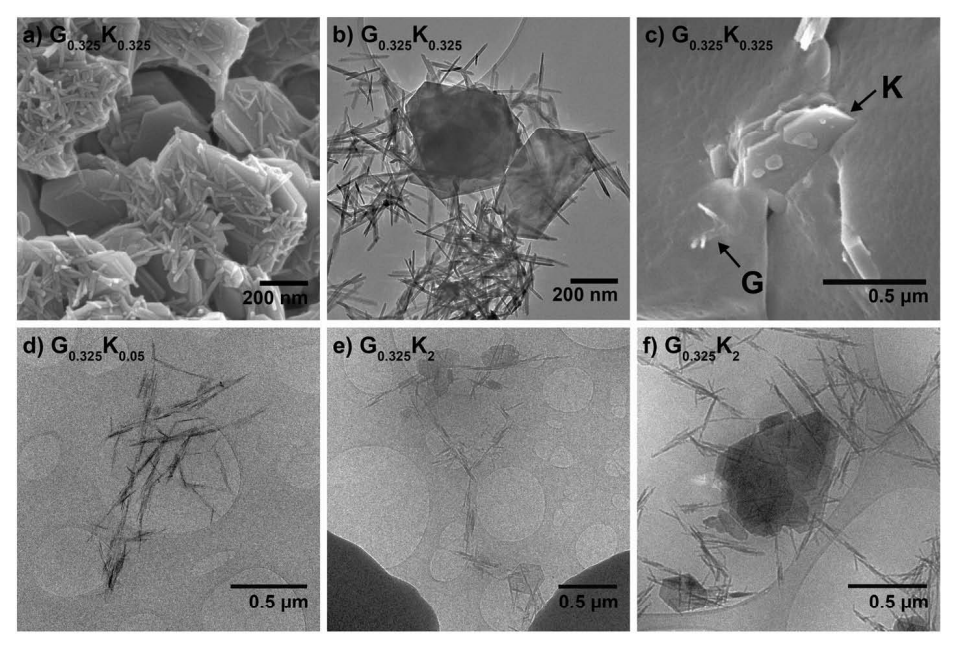


Fig. 2 Images of goethite (G) and kaolinite (K) mixed-mineral suspensions in 10 mM bicarbonate buffer at pH 7 using microscopic techniques at different mass loadings. (a-c) Goethite and kaolinite (0.325 g L^{-1} of each) taken by a) SEM, b) TEM, and c) cryo-SEM. (d) Cryo-TEM image of 0.325 g L^{-1} goethite and 0.05 g L^{-1} kaolinite. (e and f) Cryo-TEM images of 0.325 g L^{-1} goethite and 2 g L^{-1} kaolinite taken of the same grid at two different locations and magnifications. For cryogenic microscopy, the particles were trapped in background matrices of vitrified water for cryo-TEM and ice for cryo-SEM. Sample notation indicates the mass loading of goethite or kaolinite in g L⁻¹.

considerable heteroaggregation occurred, conventional microscopy cannot directly reveal particle aggregates in their native state due to drying artifacts, such as aggregation induced from the removal of the solvent.³⁹ Thus, the application of cryogenic techniques was critical to assessing the aggregation state in liquid medium.

Extensive heteroaggregation was not observed via cryo-SEM (Fig. 2c) or cryo-TEM (Fig. 2d-f). The vast majority of goethite particles resided in homoaggregates of similar densities in all mixed mineral suspensions, independent of the kaolinite particle loading. It should be noted that kaolinite was not detected in mixed mineral suspensions containing goethite with 0.05 g L⁻¹ kaolinite (Fig. 2d). Thus, there is minimal loss of reactive goethite surface area due to heteroaggregation. Despite the comparatively large size of the kaolinite particles, cryo-TEM proved to be the superior method for characterizing the aggregation state in the mixed mineral suspensions. The SEM was not equipped with energy-dispersive X-ray spectroscopy (EDS), making particle morphology and size the only two identifiers available to distinguish the larger kaolinite platelets and goethite acicular nanoparticles from the surrounding matrix. In cryo-TEM, kaolinite was distinguished from hexagonal ice formations by purposeful beam damage (examples in Fig. S3†). In conclusion, competitive Fe(II) adsorption is the only cause with substantive evidence to explain the decreasing 4-ClNB reduction rates with increasing kaolinite particle loading during singlespike reactions.

Long-term effects of kaolinite dissolution on reactive goethite crystal faces

Kaolinite dissolution had a greater effect on $Fe(\pi)$ /goethite reactivity in the sequential-spike reactions, leading to decreas-

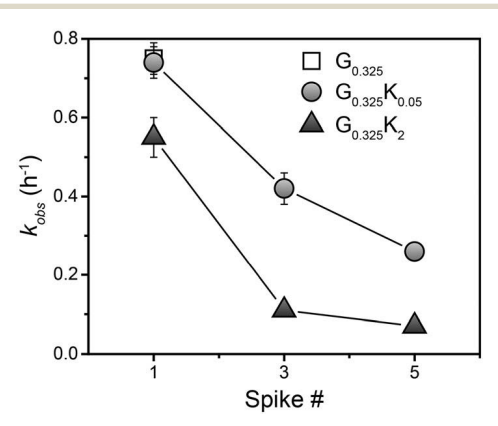


Fig. 3 Pseudo first-order reduction rates of 4-ClNB in reactors containing goethite (0.325 g L^{-1}) and various loadings of kaolinite (0, 0.05, or 2 g L^{-1}) as a function of the number of 4-ClNB spikes in 10 mM bicarbonate buffer at pH 7 and initial Fe(II) concentration of 1 mM. Sample notation indicates the mass loading of goethite (G) or kaolinite (K) in g L^{-1} . Only one 4-ClNB spike was performed for reactors containing only goethite ($G_{0.325}$). Previous work has described sequential-spike reactivity of goethite in identical conditions and in the absence of kaolinite. ⁴⁶

ing reaction rates with each 4-ClNB spike (Fig. 3, $k_{\rm obs}$ values provided in Table 1). We have previously demonstrated that, in identical conditions but in the absence of kaolinite, reduction rates did not decrease with the number of 4-ClNB spikes. ⁴⁶ The presence of kaolinite, therefore, is the responsible factor for the decreasing rates.

More specifically, kaolinite dissolution and the release of Al and Si ions resulted in the decreased 4-ClNB reduction rates by adsorbed Fe(II) on goethite. Increasing Al and Si concentrations were detected in the filtrates (Table 1) with increasing reaction spikes as well as in the digested goethite solids that were separated from kaolinite by a dialysis membrane during reaction (0.6 wt% Si and 0.2 wt% Al). The similar ionic radii of Al and Fe(III) (0.67 and 0.78 Å, respectively³⁰) suggest that Al could substitute into the goethite crystal structure, and aluminous goethite is known to occur naturally and can be synthesized. 29,50,51 Although the ionic size of Si (0.54 Å) is smaller than that of Al, its incorporation into the octahedral sites of goethite during particle growth has also been noted. 30,52 In all of these studies, the properties of Al- or Si-goethite differed from its unsubstituted counterpart, depending on the extent of isomorphic substitution. Given that Al and Si were detected in the reacted goethite solids, Al and Si incorporation into or adsorption onto the goethite surface affected the surface chemistry of the mineral and, therefore, its surface-mediated reactions with Fe(II) and 4-ClNB.

Si and Al incorporation or adsorption onto goethite is further supported by quantitative analysis of oxidative mineral growth, or formation of new goethite from produced Fe(III) on the existing particles. Oxidative growth occurred preferentially on certain goethite crystal faces depending on the amount of kaolinite initially present. Using TEM images (Fig. 4), quantification of growth on the tips and sides of goethite supported increasing growth on the {021} tip crystal faces with increasing reaction spikes (Fig. 5, averages and standard deviations provided in Table 1). Goethite particles in contact with 2 g L⁻¹ kaolinite, however, grew relatively less long and significantly more wide with each 4-ClNB spike as compared to goethite particles in contact with 0.05 g L⁻¹ kaolinite. No evidence of nucleation of new particles was seen in conventional TEM images and no magnetic transitions indicative of other iron oxide mineral phases were present in magnetic analyses (Fig. S4†) of solids after five spikes of 4-ClNB, meaning oxidative growth of goethite particles was the only product of Fe(III) formation during 4-ClNB reduction.

When normalized to initial particle size, goethite growth on the side facets was more pronounced in the presence of 2 g L^{-1} kaolinite than in conditions with decreased $Fe(\pi)$ concentration (shown in our recent work⁴⁶). Thus, the Si and Al ion species are mainly responsible for the change in relative reactivities of goethite facets. It has been shown that acicular goethite nanoparticles with 2.5 mole% Si were shorter in length as compared to goethite with no Si substitution, with preferential adsorption of Si ions occurring on the tips of the goethite.³⁰ Similar variations in goethite nanoparticle

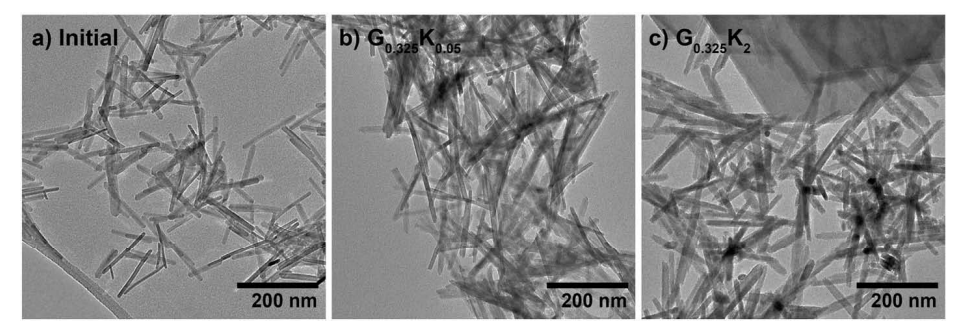


Fig. 4 Representative TEM images of 0.325 g L^{-1} goethite nanoparticles in 10 mM bicarbonate buffer at pH 7 either a) before reaction with 4-ClNB or b and c) after five spikes of 4-ClNB. b) 0.05 g L^{-1} kaolinite. c) 2 g L^{-1} kaolinite. Sample notation indicates the mass loading of goethite (G) or kaolinite (K) in $q L^{-1}$.

morphology have been observed for Al-substituted goethite, with more Al substitution resulting in shorter and wider nanoparticles.⁵³ Thus, isomorphic Al and Si substitution likely occurred simultaneously with oxidative goethite growth during these sequential-spike reactions. Because oxidative goethite growth is favorable on {021} faces,⁵⁴ those reactive sites may be initially susceptible to Al or Si incorporation. On the other hand, Si and Al incorporation or adsorption could be preferential on the {021} faces due to crystallographic constraints, as was seen for Si on goethite nanoparticles in Quin et al. 30 In both scenarios, reactive sites on the goethite tips would be sequestered and oxidative growth on the side faces of goethite would occur more than on goethite in the absence of dissolved Al or Si ions.

The results of the sequential-spike reactions provide further evidence that even trace or slowly occurring changes in ionic composition and strength of aqueous media may vary the surface chemistry and reactivity of iron oxides in groundwater systems. In addition, these results emphasize the im-

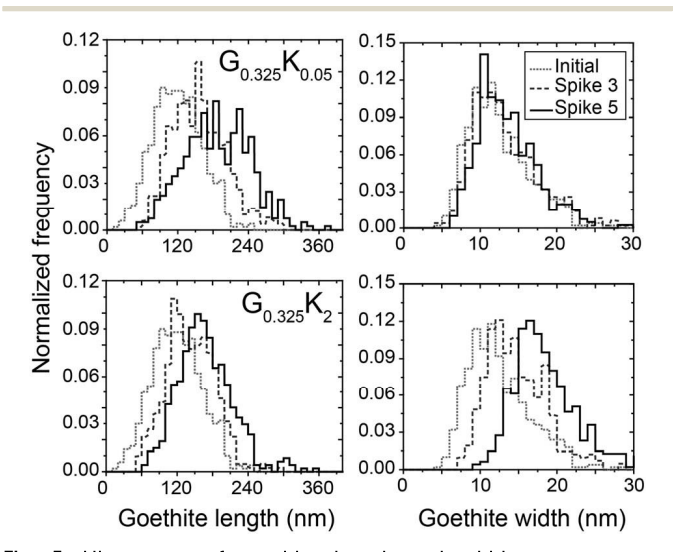


Fig. 5 Histograms of goethite length and width measurements, normalized to the number of particles measured, in suspension with either 0.05 or $2~g~L^{-1}$ kaolinite before reaction (initial), after three spikes of 4-CINB, and after five spikes of 4-CINB in 10 mM bicarbonate buffer at pH 7 and 1 mM initial Fe(II). Sample notation indicates the mass loading of goethite (G) or kaolinite (K) in g L^{-1} .

portance of including long-term studies when interpreting iron oxide reactivity in natural systems. Kaolinite dissolution, which led to Al and Si incorporation during oxidative growth, declining reaction rates, and variable goethite particle dimensions, was only observed after additional spikes of 4-ClNB were performed. Consideration of the variable particle dimensions following redox reactions with contaminants is especially important for current models predicting the transport of nanoparticles in environmental systems.

Conclusion

The presence of nonreactive clay minerals, such as kaolinite, affects the surface-mediated reactions of Fe(II) on iron oxides with NACs in groundwater systems. Fe(II) on kaolinite was not an effective reductant for 4-ClNB. Instead, kaolinite initially served as a competitor for Fe(II) adsorption, increasing competition for reactive sites on goethite and slowing 4-ClNB reduction rates. Cryo-TEM images of a clay and iron oxide mixed-mineral suspension in dilute aqueous conditions revealed that heteroaggregation did not affect the accessibility of goethite reactive sites at the explored particle loadings. Kaolinite dissolution had a greater effect on the Fe(II)/goethite system during reactions of longer periods, especially at higher kaolinite loadings. As a result, reactive sites were inhibited and 4-ClNB reduction rates slowed considerably with time. In addition, the incorporation of Al and Si varied the chemistry of the goethite crystal faces, sequestering goethite tip reactive sites and promoting oxidative growth on side crystal faces.

Clays that are nonreactive towards oxidized molecules should not be assumed as passive minerals during interpretations of iron cycling in environmental systems. In other nonreactive clay and iron oxide systems, competitive Fe(II) adsorption, heteroaggregation, and/or clay dissolution may be more significant. These interactions could impact the accessible surface area as well as the transport properties of iron oxides more so than the kaolinite-goethite mixed-mineral suspensions studied here. In addition, the extent of isomorphic substitution or crystal defects in kaolinite, or another nonreactive clay, as well as in the iron oxides themselves greatly change the chemical and physical properties of the

minerals.^{55,56} Further investigations and microscopic analyses of evolving reactivity in Al- and Si-substituted iron oxide suspensions and in varying Al and Si concentrations will elucidate the specific mechanisms defining the relative reactivity of each goethite crystal face.

Acknowledgements

This work was funded by NSF grants ECS-1012193 and CHE-1507496 (R. L. P. and W. A. A.), the Graduate School Doctoral Dissertation Fellowship at the University of Minnesota (J. H. S.), and the Undergraduate Research Opportunity Program (UROP) at the University of Minnesota (J. D. S.). Cryo-SEM was performed with the invaluable assistance of Chris Frethem (Characterization Facility, University of Minnesota). Magnetic characterization was performed at the Institute for Rock Magnetism (IRM) at the University of Minnesota with support from Becky E. Strauss, Joshua M. Feinberg, and Mike Jackson. The IRM is a US National Multi-user Facility supported through the Instrumentation and Facilities program of the National Science Foundation, Earth Sciences Division, and by funding from the University of Minnesota. Analyses by ICP-OES were performed by Rick Knurr with the Analytical Geochemistry Lab, part of the Department of Earth Sciences at the University of Minnesota. Parts of this work were carried out in the Characterization Facility, University of Minnesota, a member of the NSF-funded Materials Research Facilities Network (www.mrfn.org) via the MRSEC program.

References

- 1 J. Klausen, S. P. Tröber, S. B. Haderlein and R. P. Schwarzenbach, Reduction of substituted nitrobenzenes by Fe(II) in aqueous mineral suspensions, *Environ. Sci. Technol.*, 1995, 29, 2396–2404.
- 2 T. B. Hofstetter, C. G. Heijman, S. B. Haderlein, C. Holliger and R. P. Schwarzenbach, Complete reduction of TNT and other (poly)nitroaromatic compounds under iron-reducing subsurface conditions, *Environ. Sci. Technol.*, 1999, 33, 1479–1487.
- 3 T. P. Klupinski, Y.-P. Chin and S. J. Traina, Abiotic degradation of pentachloronitrobenzene by Fe(II): Reactions on goethite and iron oxide nanoparticles, *Environ. Sci. Technol.*, 2004, 38, 4353–4360.
- 4 A. G. B. Williams and M. M. Scherer, Spectroscopic evidence for Fe(II)-Fe(III) electron transfer at the iron oxide-water interface, *Environ. Sci. Technol.*, 2004, 38, 4782–4790.
- 5 M. E. Essington, *Soil and Water Chemistry: An Integrative Approach*, CRC Press, Boca Raton, FL, 2004.
- 6 M. Elsner, R. P. Schwarzenbach and S. B. Haderlein, Reactivity of Fe(II)-bearing minerals toward reductive transformation of organic contaminants, *Environ. Sci. Technol.*, 2004, 38, 799–807.
- 7 T. B. Hofstetter, R. P. Schwarzenbach and S. B. Haderlein, Reactivity of Fe(II) species associated with clay minerals, *Environ. Sci. Technol.*, 2003, 37, 519–528.

- 8 M. V. Schaefer, C. A. Gorski and M. M. Scherer, Spectroscopic evidence for interfacial Fe(II)-Fe(III) electron transfer in a clay mineral, *Environ. Sci. Technol.*, 2011, 45, 540–545.
- 9 T. B. Hofstetter, A. Neumann and R. P. Schwarzenbach, Reduction of nitroaromatic compounds by Fe(II) species associated with iron-rich smectites, *Environ. Sci. Technol.*, 2006, 40, 235–242.
- 10 A. Neumann, T. B. Hofstetter, M. Skarpeli-Liati and R. P. Schwarzenbach, Reduction of polychlorinated ethanes and carbon tetrachloride by structural Fe(II) in smectites, *Environ. Sci. Technol.*, 2009, 43, 4082–4089.
- 11 F. Luan, Y. Liu, A. M. Griffin, C. A. Gorski and W. D. Burgos, Iron(III)-bearing clay minerals enhance bioreduction of nitrobenzene by *Shewanella putrefaciens* CN32, *Environ. Sci. Technol.*, 2015, 49, 1418–1426.
- 12 A. Neumann, T. L. Olson and M. M. Scherer, Spectroscopic evidence for Fe(II)-Fe(III) electron transfer at clay mineral edge and basal sites, *Environ. Sci. Technol.*, 2013, 47, 6969–6977.
- 13 A. Neumann, L. Wu, W. Li, B. L. Beard, C. M. Johnson, K. M. Rosso, A. J. Frierdich and M. M. Scherer, Atom exchange between aqueous Fe(II) and structural Fe in clay minerals, *Environ. Sci. Technol.*, 2015, 49, 2786–2795.
- 14 C. A. Gorski, L. E. Klupfel, A. Voegelin, M. Sander and T. B. Hofstetter, Redox properties of structural Fe in clay minerals: 3. Relationships between smectite redox and structural properties, *Environ. Sci. Technol.*, 2013, 47, 13477–13485.
- 15 C. A. Gorski, M. Aeschbacher, D. Soltermann, A. Voegelin, B. Baeyens, M. M. Fernandes, T. B. Hofstetter and M. Sander, Redox properties of structural Fe in clay minerals. 1. Electrochemical quantification of electron-donating and accepting capacities of smectites, *Environ. Sci. Technol.*, 2012, 46, 9360–9368.
- 16 C. A. Gorski, L. Klupfel, A. Voegelin, M. Sander and T. B. Hofstetter, Redox properties of structural Fe in clay minerals.
 2. Electrochemical and spectroscopic characterization of electron transfer irreversibility in ferruginous smectite, SWa-1, *Environ. Sci. Technol.*, 2012, 46, 9369–9377.
- 17 A. Neumann, M. Sander and T. B. Hofstetter, Redox properties of structural Fe in smectite clay minerals, in *Aquatic Redox Chemistry*, ed. P. G. Tratnyek, T. J. Grundl and S. B. Haderlein, American Chemical Society, Washington, D. C., 2011, pp. 361–379.
- 18 H. Li, B. J. Teppen, C. T. Johnston and S. A. Boyd, Thermodynamics of nitroaromatic compound adsorption from water by smectite clay, *Environ. Sci. Technol.*, 2004, 38, 5433-5442.
- 19 C. T. Johnston, M. Fernandes de Oliveira, B. J. Teppen, G. Sheng and S. A. Boyd, Spectroscopic study of nitroaromatic smectite sorption mechanisms, *Environ. Sci. Technol.*, 2001, 35, 4767–4772.
- 20 S. A. Boyd, G. Sheng, B. J. Teppen and C. T. Johnston, Mechanisms for the adsorption of substituted nitrobenzenes by smectite clays, *Environ. Sci. Technol.*, 2001, 35, 4227–4234.

- 21 S. B. Haderlein and R. P. Schwarzenbach, Adsorption of substituted nitrobenzenes and nitrophenols to mineral surfaces, *Environ. Sci. Technol.*, 1993, 27, 316–326.
- 22 S. B. Haderlein, K. W. Weissmahr and R. P. Schwarzenbach, Specific adsorption of nitroaromatic explosives and pesticides to clay minerals, *Environ. Sci. Technol.*, 1996, 30, 612–622.
- 23 K. G. Bhattacharyya and S. S. Gupta, Adsorption of a few heavy metals on natural and modified kaolinite and montmorillonite: A review, *Adv. Colloid Interface Sci.*, 2008, **140**, 114–131.
- 24 I. J. Buerge and S. J. Hug, Influence of mineral surfaces on chromium(VI) reduction by iron(II), *Environ. Sci. Technol.*, 1999, 33, 4285-4291.
- 25 A. Ioannou and A. Dimirkou, Phosphate adsorption on hematite, kaolinite, and kaolinite-hematite (k-h) systems as described by a constant capacitance model, *J. Colloid Interface Sci.*, 1997, 192, 119–128.
- 26 S. Wei, W. Tan, F. Liu, W. Zhao and L. Weng, Surface properties and phosphate adsorption of binary systems containing goethite and kaolinite, *Geoderma*, 2014, 213, 478-484.
- 27 T. J. Reich, S. Das, C. M. Koretsky, T. J. Lund and C. J. Landry, Surface complexation modeling of Pb(II) adsorption on mixtures of hydrous ferric oxide, quartz and kaolinite, *Chem. Geol.*, 2010, 275, 262–271.
- 28 S. A. Carroll-Webb and J. V. Walther, A surface complex reaction model for the pH-dependence of corundum and kaolinite dissolution rates, *Geochim. Cosmochim. Acta*, 1988, 52, 2609–2623.
- 29 D. E. Latta, J. E. Bachman and M. M. Scherer, Fe electron transfer and atom exchange in goethite: Influence of Alsubstitution and anion sorption, *Environ. Sci. Technol.*, 2012, 46, 10614–10623.
- 30 T. G. Quin, G. J. Long, C. G. Benson, S. Mann and R. J. P. Williams, Influence of silicon and phosphorus on structural and magnetic properties of synthetic goethite and related oxides, *Clays Clay Miner.*, 1988, 36, 165–175.
- 31 A. M. Jones, A. S. Kinsela, R. N. Collins and T. D. Waite, The reduction of 4-chloronitrobenzene by Fe(II)-Fe(III) oxide systems correlations with reduction potential and inhibition by silicate, *J. Hazard. Mater.*, 2016, 320, 143–149.
- 32 A. J. Frierdich, M. M. Scherer, J. E. Bachman, M. H. Engelhard, B. W. Rapponotti and J. G. Catalano, Inhibition of trace element release during Fe(II)-activated recrystallization of Al-, Cr-, and Sn-substituted goethite and hematite, *Environ. Sci. Technol.*, 2012, 46, 10031–10039.
- 33 P. Joshi and C. A. Gorski, Anisotropic morphological changes in goethite during Fe²⁺-catalyzed recrystallization, *Environ. Sci. Technol.*, 2016, **50**, 7315–7324.
- 34 E. Tombácz, C. Csanaky and E. Illés, Polydisperse fractal aggregate formation in clay mineral and iron oxide suspensions, pH and ionic strength dependence, *Colloid Polym. Sci.*, 2001, 279, 484–492.
- 35 T. Hou, R. Xu and A. Zhao, Interaction between electric double layers of kaolinite and Fe/Al oxides in suspensions, *Colloids Surf.*, A, 2007, 297, 91–94.

- 36 A. Dimirkou, A. Ioannou and M. Doula, Preparation, characterization and sorption properties for phosphates of hematite, bentonite and bentonite-hematite systems, *Adv. Colloid Interface Sci.*, 2002, 97, 37–61.
- 37 B. K. Schroth and G. Sposito, Surface charge properties of kaolinite, *Clays Clay Miner.*, 1997, 45, 85–91.
- 38 M. Kosmulski, Compilation of PZC and IEP of sparingly soluble metal oxides and hydroxides from literature, *Adv. Colloid Interface Sci.*, 2009, **152**, 14–25.
- 39 N. D. Burrows and R. L. Penn, Cryogenic transmission electron microscopy: aqueous suspensions of nanoscale objects, *Microsc. Microanal.*, 2013, 19, 1542–1553.
- 40 A. M. Vindedahl, W. A. Arnold and R. L. Penn, Impact of pahokee peat humic acid and buffer identity on goethite aggregation and reactivity, *Environ. Sci.: Nano*, 2015, 2, 509-517.
- 41 V. M. Yuwono, N. D. Burrows, J. A. Soltis, T. A. Do and R. L. Penn, Aggregation of ferrihydrite nanoparticles in aqueous systems, *Faraday Discuss.*, 2012, **159**, 235–245.
- 42 M. Nègre, P. Leone, J. Trichet, C. Défarge, V. Boero and M. Gennari, Characterization of model soil colloids by cryoscanning electron microscopy, *Geoderma*, 2004, 121, 1–16.
- 43 A. J. Anschutz and R. L. Penn, Reduction of crystalline iron(III) oxyhydroxides using hydroquinone: Influence of phase and particle size, *Geochem. Trans.*, 2005, 6, 60–66.
- 44 R. J. Pruett and H. L. Webb, Sampling and analysis of KGa-1B well-crystallized kaolin source clay, *Clays Clay Miner.*, 1993, 41, 514–519.
- 45 L. L. Stookey, Ferrozine a new spectrophotometric reagent for iron, *Anal. Chem.*, 1970, 42, 779–781.
- 46 J. H. Strehlau, M. S. Stemig, R. L. Penn and W. A. Arnold, Facet-dependent oxidative goethite growth as a function of aqueous solution conditions, *Environ. Sci. Technol.*, 2016, 50, 10406–10412.
- 47 F. J. Huertas, L. Chou and R. Wollast, Mechanism of kaolinite dissolution at room temperature and pressure, part II: kinetic study, *Geochim. Cosmochim. Acta*, 1999, 63, 3261–3275.
- 48 Z. Xie and J. V. Walther, Incongruent dissolution and surface area of kaolinite, *Geochim. Cosmochim. Acta*, 1992, 56, 3357–3363.
- 49 A. M. Stemig, T. A. Do, V. M. Yuwono, W. A. Arnold and R. L. Penn, Goethite nanoparticle aggregation: effects of buffers, metal ions, and 4-chloronitrobenzene reduction, *Environ. Sci.: Nano*, 2014, 1, 478–487.
- 50 D. Schulze, G. The influence of aluminum on iron oxides. VIII. Unit-cell dimensions of Al-substituted goethites and estimation of Al from them, *Clays Clay Miner.*, 1984, 32, 36–44.
- 51 H. Liu, T. Chen, R. L. Frost, D. Chang, C. Qing and Q. Xie, Effect of aging time and Al substitution on the morphology of aluminous goethite, *J. Colloid Interface Sci.*, 2012, 385, 81–86.
- 52 U. Schwertmann and R. M. Taylor, The influence of silicate on the transformation of lepidocrocite to goethite, *Clays Clay Miner.*, 1972, **20**, 159–164.

- 53 D. G. Schulze and U. Schwertmann, The influence of aluminium on iron oxides: X. Properties of Al-substituted goethites, *Clay Miner.*, 1984, 19, 521–539.
- 54 C. L. Chun, R. L. Penn and W. A. Arnold, Kinetic and microscopic studies of reductive transformations of organic contaminants on goethite, *Environ. Sci. Technol.*, 2006, 40, 3299–3304.
- 55 C.-I. Fialips, S. Petit, A. Decarreau and D. Beaufort, Influence of synthesis pH on kaolinite "crystallinity" and surface properties, *Clays Clay Miner.*, 2000, 48, 173–184.
- 56 S. Petit, J. Madejová, A. Decarreau and F. Martin, Characterization of octahedral substitutions in kaolinites using near infrared spectroscopy, *Clays Clay Miner.*, 1999, 47, 103–108.